Supporting information for

Interphasic Separation of *cis*/*trans* Perylene-Based Nanographene Isomers Driven by Selective Encapsulation in a Supramolecular Cage

Carles Fuertes-Espinosa,* Clara Sabrià, Judith Sala, Lorena Capdevila, Ferran Feixas, and Xavi Ribas*

I. Supplementary experimental procedures

1. General Methods

Commercial reagents and solvents: All chemicals and solvents were purchased from commercial suppliers unless otherwise stated.

Synthesized reagents: G-**1,** G-**2,** G-**3** and **4**·$(BArF)_8$ were synthesized according to reported literature procedures and characterized using routine characterization techniques. [1, 2]

Synthesis and purification: Standard techniques were used, employing nitrogen as the inert gas when required. If they were not performed at room temperature, the reaction temperatures refer to the temperature of the heating/cooling bath. TLC analysis was done on Merck silica gel 60 F_{254} aluminum sheets, and compounds were visualized with a UV lamp (254 nm or 365 nm).

NMR:

Full characterization of the newly synthesized host-guest compounds was performed using a Bruker 400 MHz Avance III HD Smart Probe spectrometer. NMR spectra for routine ^1H NMR, ^1H DOSY and host-guest ^1H NMR titration were recorded using a Bruker 400 MHz Avance III HD Smart Probe. Chemical shifts (δ) are given in parts per million (ppm) relative to TMS, using the solvent residual peak as internal standard (CD_2Cl_2: δ = 5,29 for ^1H, δ = 77.16 for ^{13}C, Acetonitrile-d_3: δ = 1.94 for ^1H). Data is reported as follows: chemical shifts (δ) in ppm, multiplicity (s = singlet, d = doublet, dd = doublet of doublets, ddd = doublet of doublets of doublets, t = triplet, q = quartet, m = multiplet), coupling constants *J* (Hz), and integration. Signals were assigned with the help of 2D NMR experiments.

High-resolution mass (HMRS) spectra were recorded on a Bruker MicroTOF-Q-II.

II. Molecular Dynamics Simulations:

The parametrization of the supramolecular cage **4**·Cl_8 was derived from our previous work.[3] The force-field parameters of the cage were obtained using a protocol combining the General Amber Force Field (GAFF)[4] and the Metal Center Parameter Builder (MCPB.py)[5] tool, using the X-ray data as the starting structure. See Supporting Information of reference 3 for a complete description of the parametrization strategy and parameters of cage **4**·Cl_8. Parameters for the nanographenes were generated within the antechamber module using GAFF, with partial charges set to fit the electrostatic potential generated at the B3LYP/6-31G* level by the RESP model.[6] The charges were calculated according to the Merz-Singh-Kollman using the Gaussian 16 package.[7]

Molecular dynamics (MD) simulations were carried out using acetonitrile (MeCN) as solvent and the GPU code (pmemd)[8] of the AMBER 18 package.[9] The nanographenes were manually placed inside the cavity of the cage as the starting point for the MD trajectories. Each host-guest system was immersed in a preequilibrated truncated octahedron box with a 10 Å buffer of MeCN molecules using the leap module, adding thousands of solvent molecules as a result. The system was neutralized by adding eight explicit counter ions (Cl^-), which serve as a module counterion for $BArF^-$. A two-stage geometry optimization approach was performed. The first stage corresponds to a minimization of the positions of solvent molecules and ions imposing positional restraints on the solute by harmonic potential with a force constant of 500 kcal mol^{-1} $Å^{-2}$. The second stage involves an unrestrained minimization of all atoms in the simulation cell. The system is heated using six 50 ps steps, where the temperature is incremented 50 K each step (0-300 K) under constant volume and periodic boundary conditions. The SHAKE algorithm was employed to constrain the covalent bonds containing hydrogens. Long-range electrostatic effects were modelled using the particle-mesh Ewald method. An 8 Å cutoff was applied to Lennard-Jones and electrostatic interactions. Harmonic restraints of 10 kcal mol^{-1} were applied to the solute, and the Langevin equilibration scheme was used to control and equalize the temperature. The time step was maintained at 2 fs during all the heating stages, allowing potential in homogeneities to self-adjust. Finally, each system was equilibrated without restraints for 2 ns with a 2 fs time step at a constant pressure of 1 atm and a temperature of 300 K. Once the equilibration stage is completed, the system is ready for long production runs. 3 replicates of 0.5 μs were performed for each system.

*NCIPLOT was used to calculate the Non-covalent interaction (NCI) volume between the cage **4**·Cl_8 and each guest along all the simulation time for one MD replicate.[10, 11] It has been calculated without considering the solvent molecules. Two files are needed, a pdb of the starting point of the simulation and a trajectory file (dcd), both without containing the ions (Cl^-) and solvent molecules (MeCN). The residue number of the ligand, which in this case corresponds to the guest molecule, has to be indicated. With cpptraj, each trajectory frame is converted to ligand (guest) and receptor (host) pdb files, which are further converted to xyz files with openbabel. Then, the NCI volume is calculated between*

the atoms of the ligand and the atoms of the receptor that are at a distance of 5 Å for each frame. The results were visualized with PyMOL using a rainbow scale and a gradient isosurface with s = 0.8 a.u., where the repulsive interactions are represented in red, the attractive interactions in blue and weak van der Waals interactions in green.

III. Characterization of G-1 ⊂ 4·$(BArF)_8$ host-guest complex

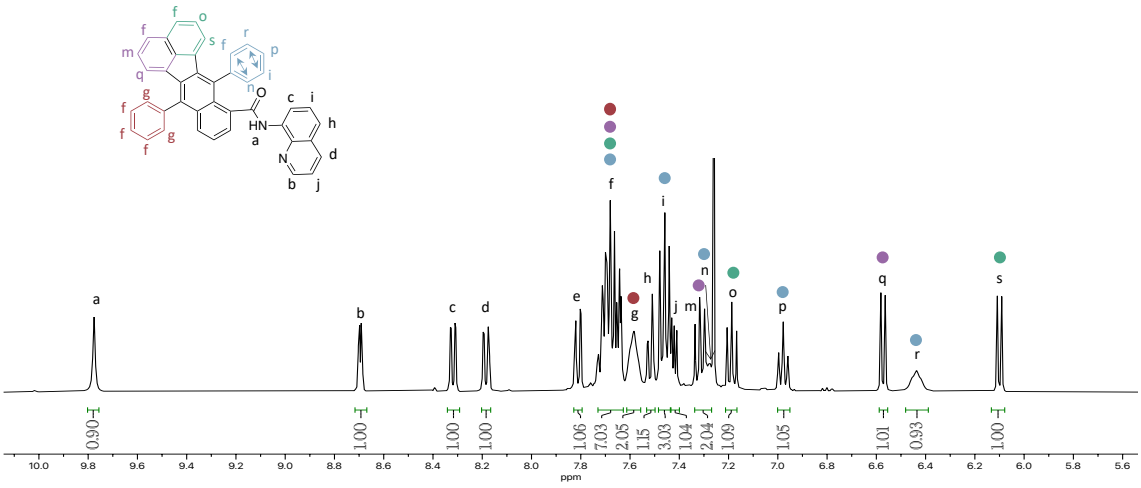

Figure S1: Partial ^{1}H NMR spectrum (400 MHz, $CDCl_3$, 298 K) of G-**1**.

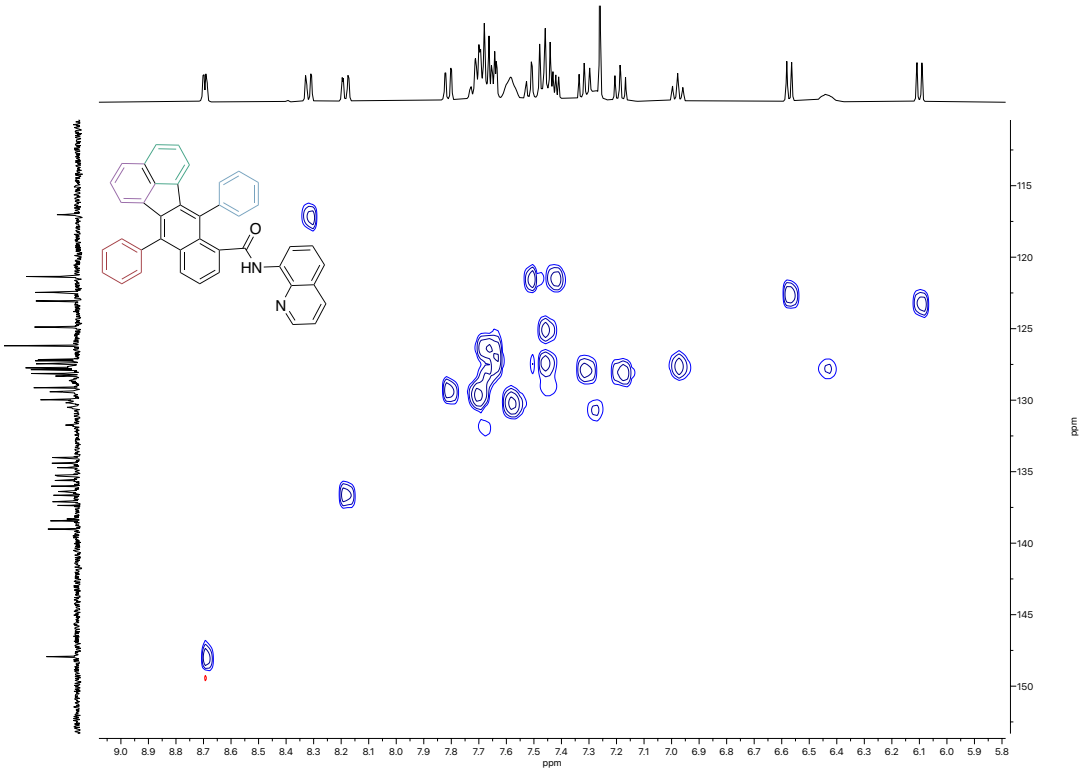

Figure S2: HSQC spectrum (400 MHz, $CDCl_3$, 298 K) of G-**1**.

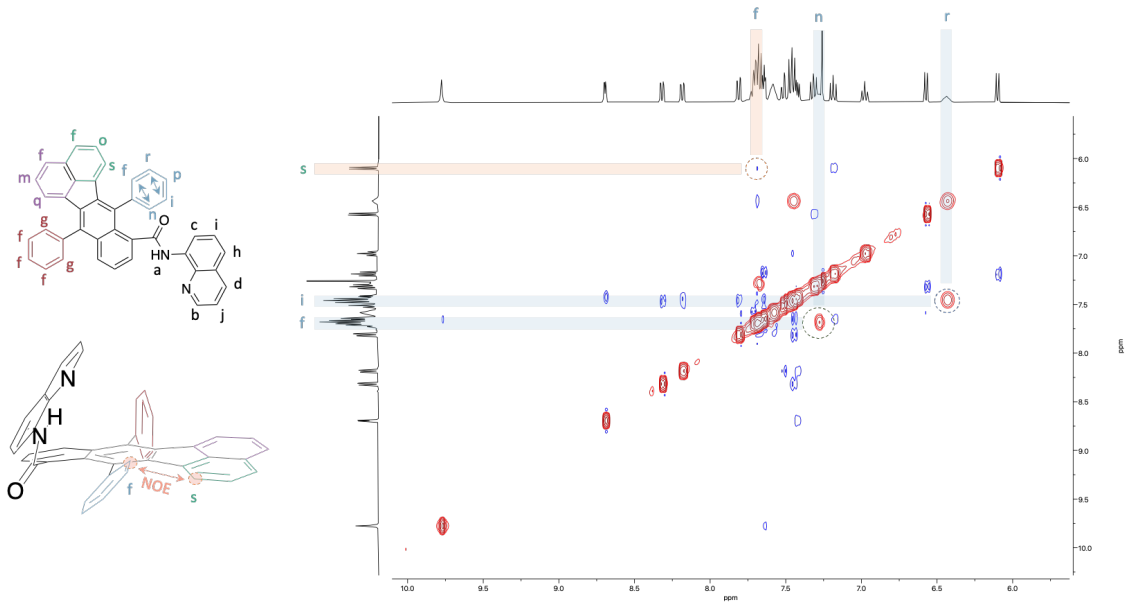

Figure S3: Two-dimensional NOESY NMR spectrum (400 MHz, $CDCl_3$, 298 K) of G-**1**.

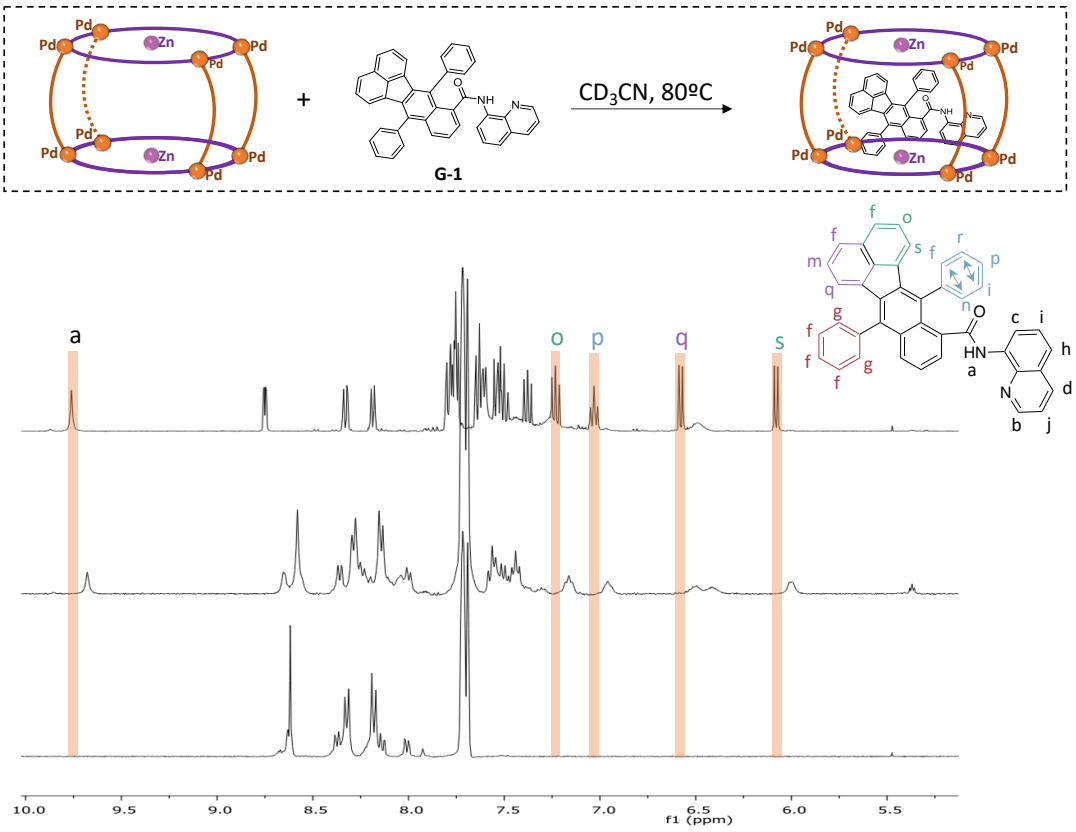

Figure S4: Stacked ^{1}H NMR spectra (400 MHz, CD_3CN, 298 K) of **4**·$(BArF)_8$ (bottom), the prepared G-**1** ⊂ **4**·$(BArF)_8$ host-guest complex (middle) and G-**1** (top).

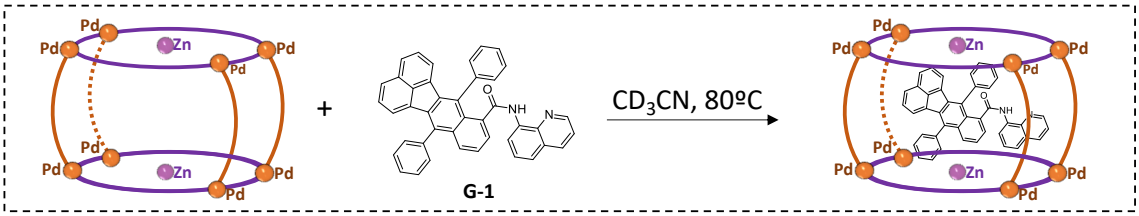

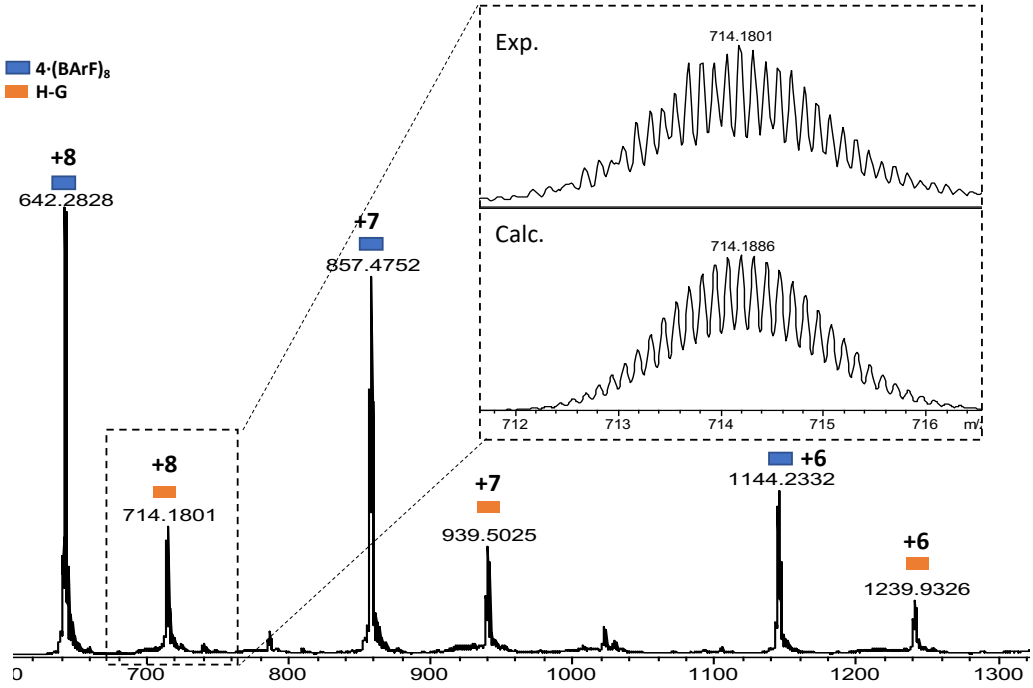

Figure S5: High Resolution Mass Spectrometry (HRMS) spectrum of G-**1** ⊂ **4**·(BArF)$_8$ host-guest complex (CH_3CN solvent).

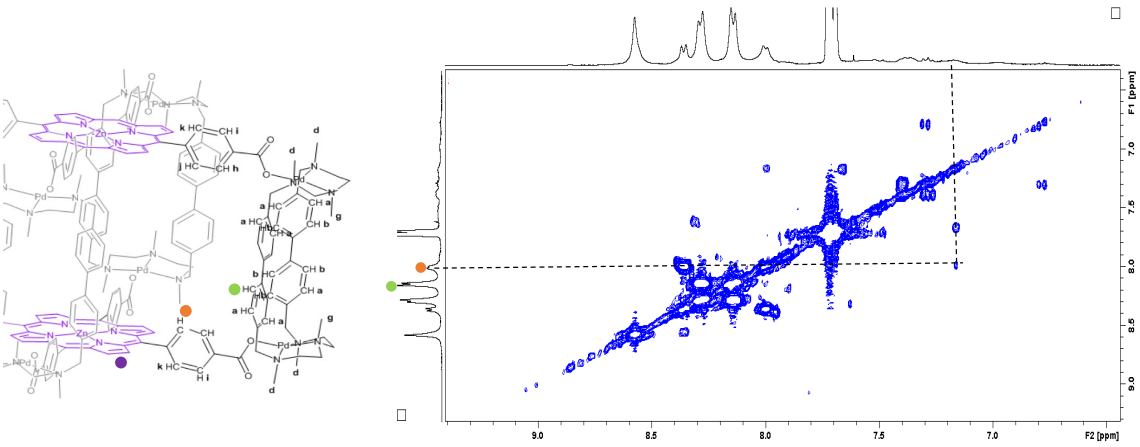

Figure S6. *Two-dimensional NOESY spectra (400 MHz, CD_3CN, 298 K) of G-**1** ⊂ **4**·(BArF)$_8$ host-guest complex. Illustration of different **4**·(BArF)$_8$ protons showing NOESY correlations. The correlations observed are attributed to the proximity of the aromatic protons of G-**1** and the aromatic protons of **4**·(BArF)$_8$ pointing inwards towards the host cavity.*

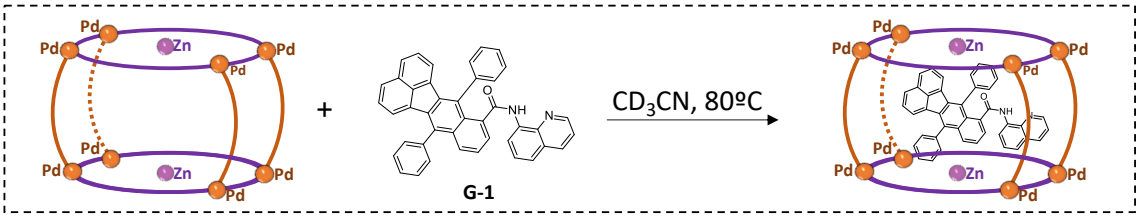

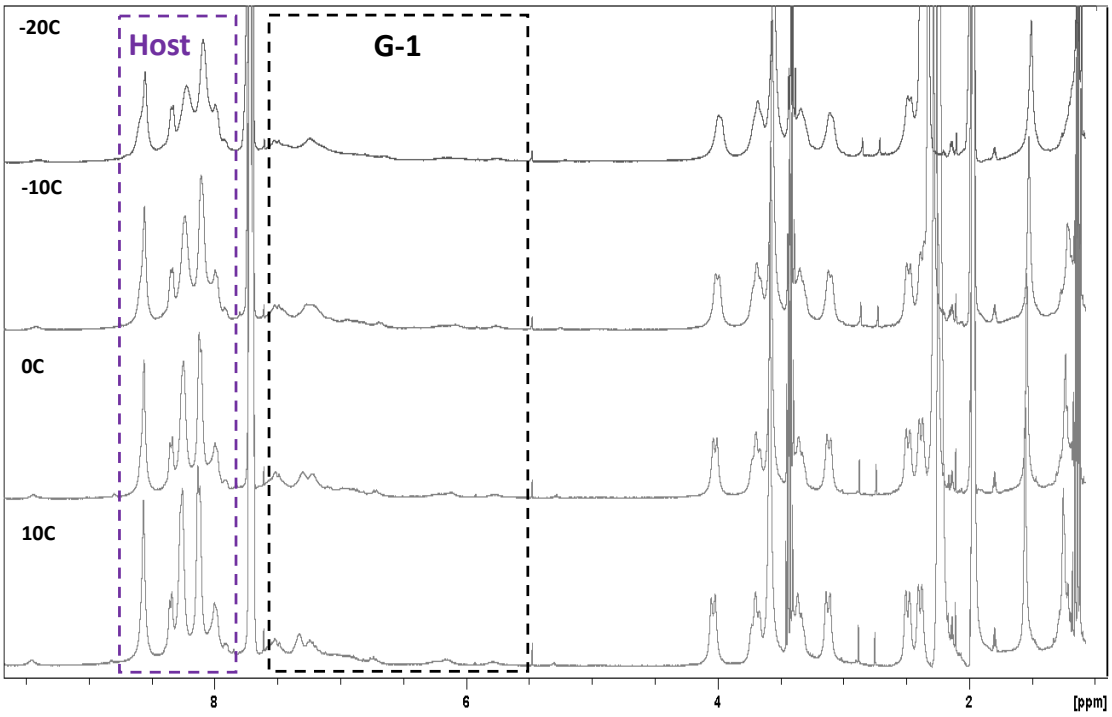

Figure S7: Stacked ^{1}H NMR spectra (400 MHz, CD_3CN) of G-**1** ⊂ **4**·$(BArF)_8$ host-guest complex, recorded at different temperatures.

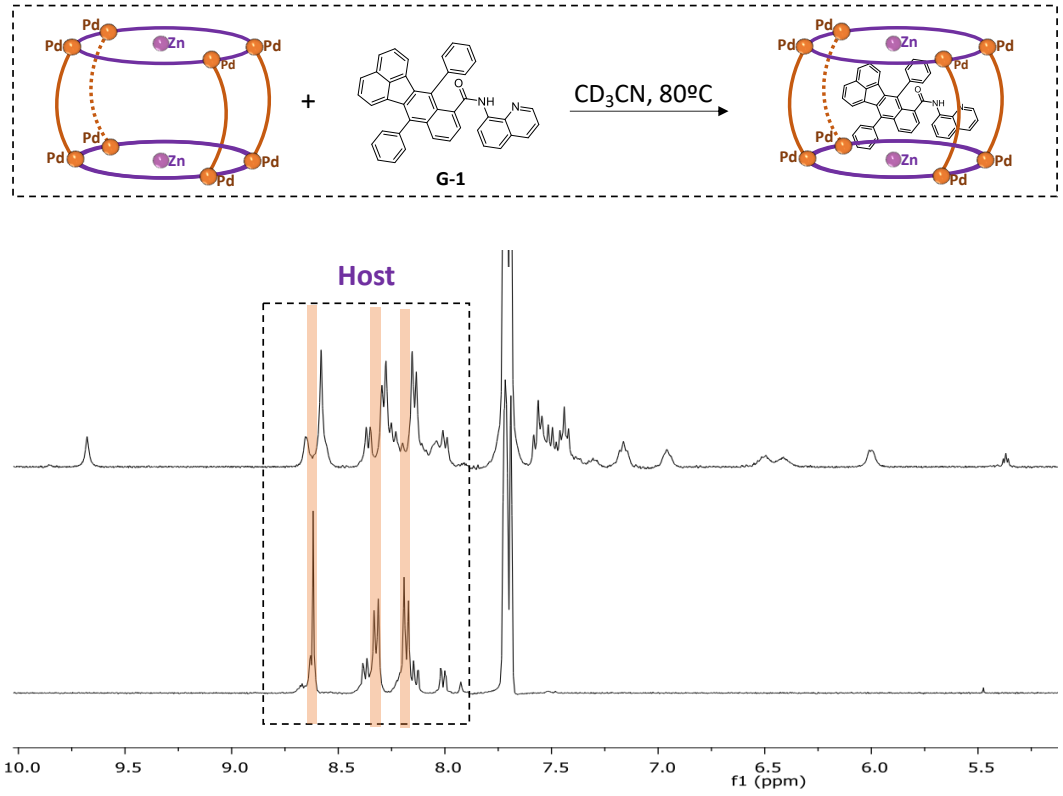

Figure S8: Stacked ^{1}H NMR spectra (400 MHz, CD_3CN) of **4**·$(BArF)_8$ (bottom) and G-**1** ⊂ **4**·$(BArF)_8$ host-guest complex (top).

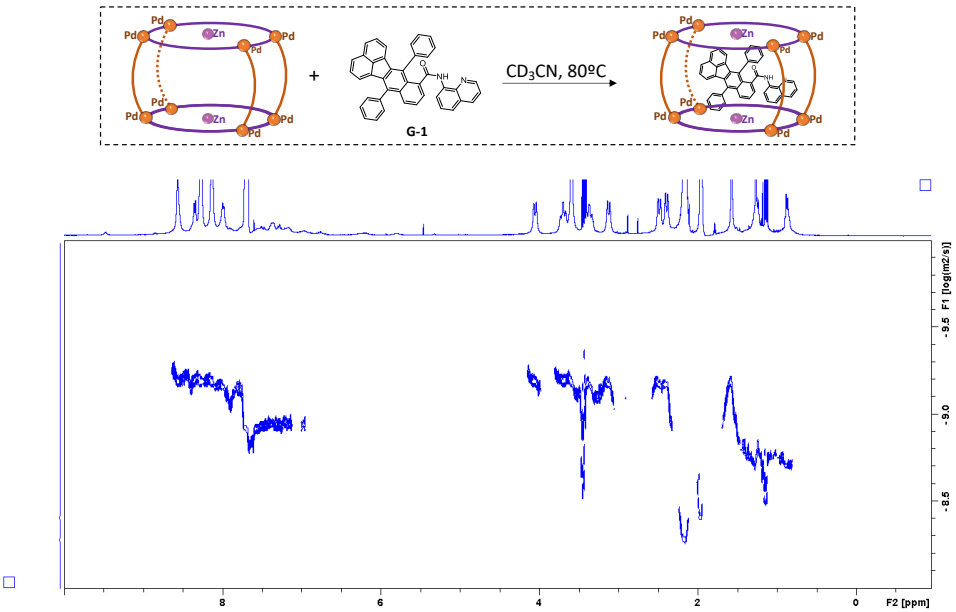

Figure S9: ^{1}H DOSY spectrum (400 MHz, CD_3CN, 298 K) of the prepared *G*-**1** ⊂ **4**·$(BArF)_8$ host-guest complex. The diffusion coefficients for the host and the guest species in the G-**1** ⊂ **4**·$(BArF)_8$ host-guest complex in CD_3CN were measured to be $D=10^{-9.414}$ m^2 $s^{-1}$and $D=10^{-8.951}$ m^2 s^{-1}, respectively. The differences observed in the diffusion coefficients of the host and the guest in the G-**1** ⊂ **4**·$(BArF)_8$ host-guest complex are indicative of fast exchange binding dynamics on the NMR time scale.

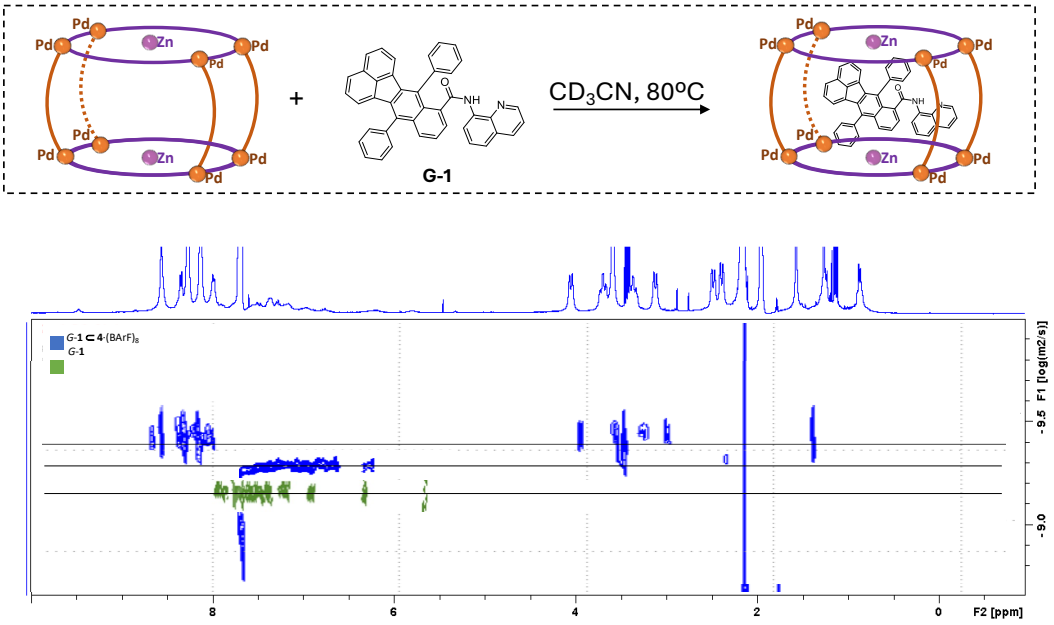

Figure S10: Overlapped ^{1}H DOSY spectra (400 MHz, CD_3CN, 298 K) of the prepared G-**1** ⊂ **4**·$(BArF)_8$ host-guest complex (red) and G-**1** (blue). The diffusion coefficient for free G-**1** in CD_3CN was measured to be $D=10^{-9.157}$ m^2 s^{-1}. The diffusion coefficients for the host and the guest species in the G-**1** ⊂ **4**·$(BArF)_8$ host-guest complex in CD_3CN were measured to be $D=10^{-9.414}$ m^2 $s^{-1}$and $D=10^{-9.298}$ m^2 s^{-1}, respectively. The differences observed in the diffusion coefficients of the guest in the host-guest complex and the free guest are indicative of the confinement of G-**1** within **4**·$(BArF)_8$.

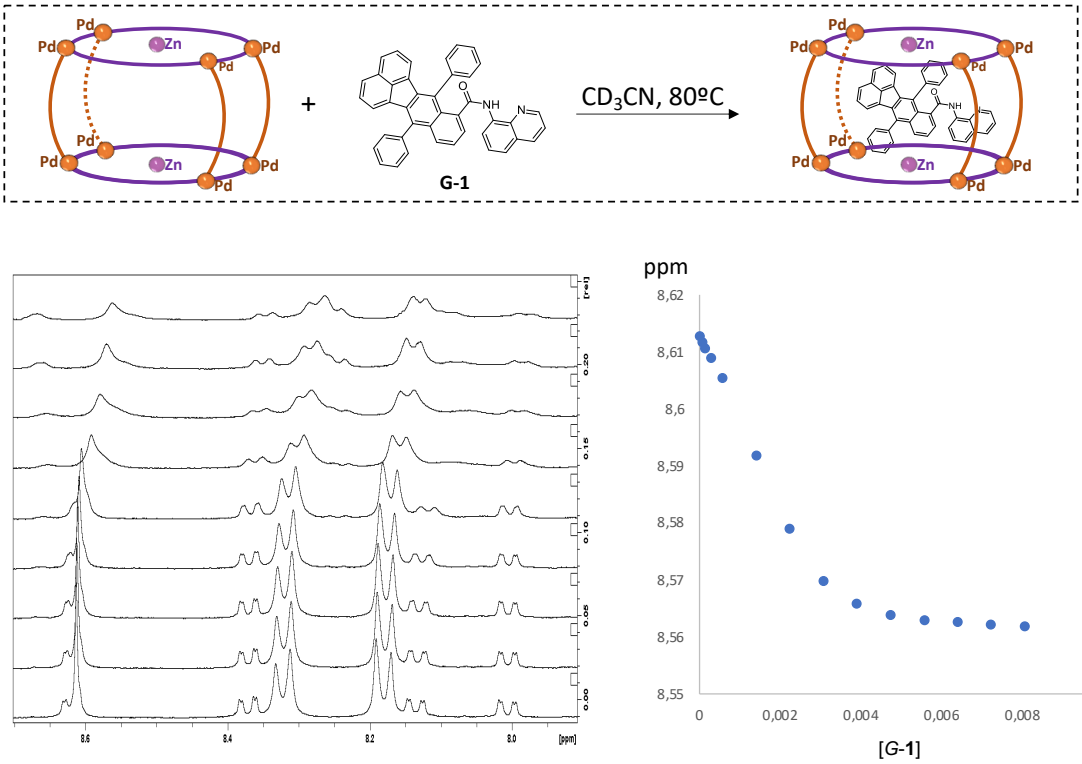

Figure S11: ^{1}H NMR (400 MHz, CD_3CN) monitoring for the titration of **4**·$(BArF)_8$ with G-**1**. Fixed total concentration of **4**·$(BArF)_8$ in acetonitrile was measured to be $8.32 \cdot 10^{-4}$ M (fitting with www.supramolecular.org, K_a = 4.03 (±0.1) × 10^4 M^{-1}). Inset: chemical shift variation of the host plotted versus the different stoichiometries of G-**1**.

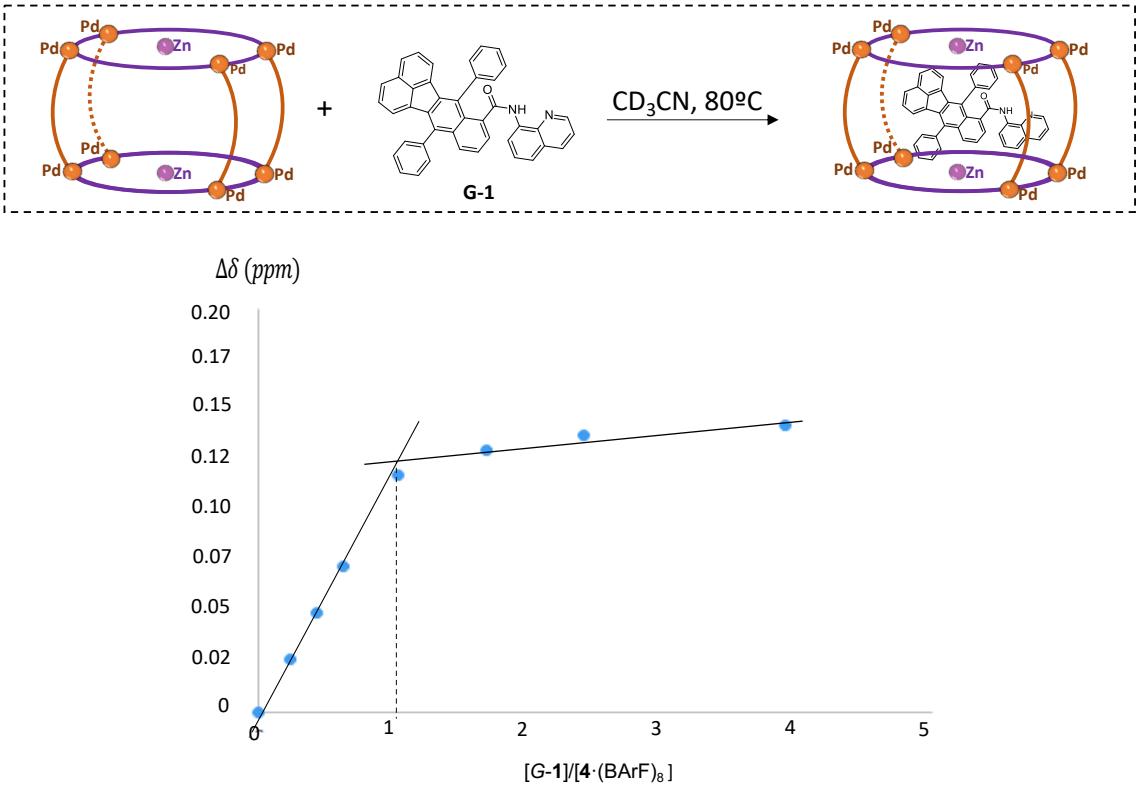

Figure S12. ^{1}H-NMR stoichiometry plot for the titration of **4**·(BArF)$_8$ with G-**1**. A series of 4 mM solutions of **4**·(BArF)$_8$ containing varying concentrations of *G*-**1**, ranging from 2.06 mM to 66 mM, were prepared. The solutions were allowed to equilibrate before they were examined by ^{1}H-NMR spectroscopy. The stoichiometry was found to be one guest molecule per one host molecule using the mole ratio method.

IV. Characterization of G-2 ⊂ 4·$(BArF)_8$ host-guest complex

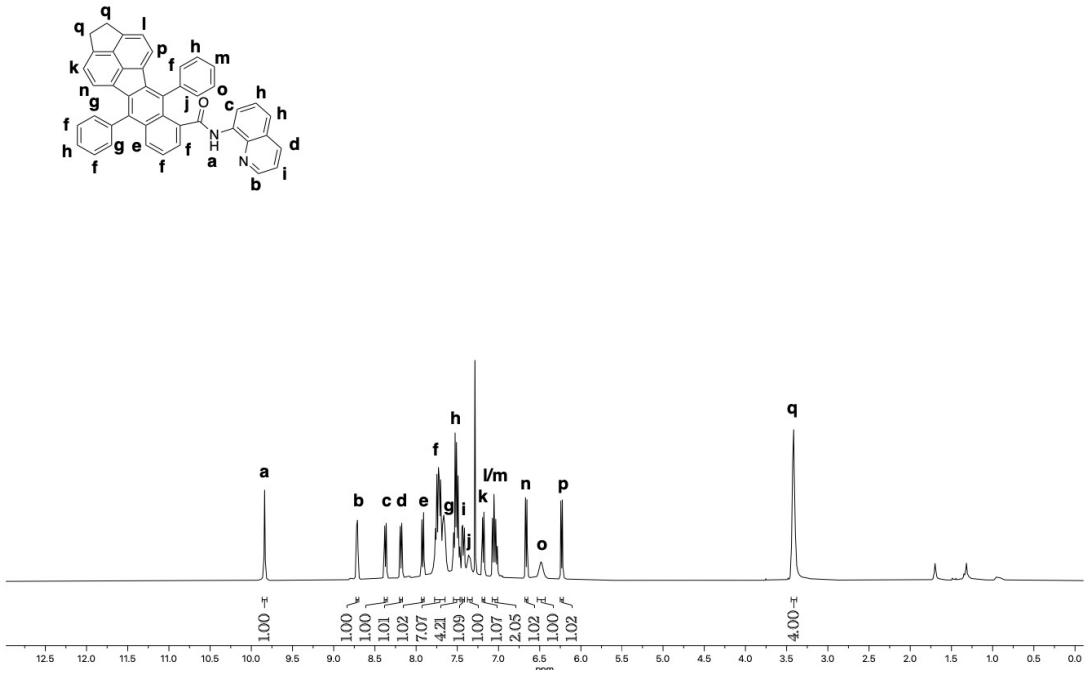

Figure S13: ^{1}H NMR spectrum (400 MHz, $CDCl_3$, 298 K) of G-**2**.

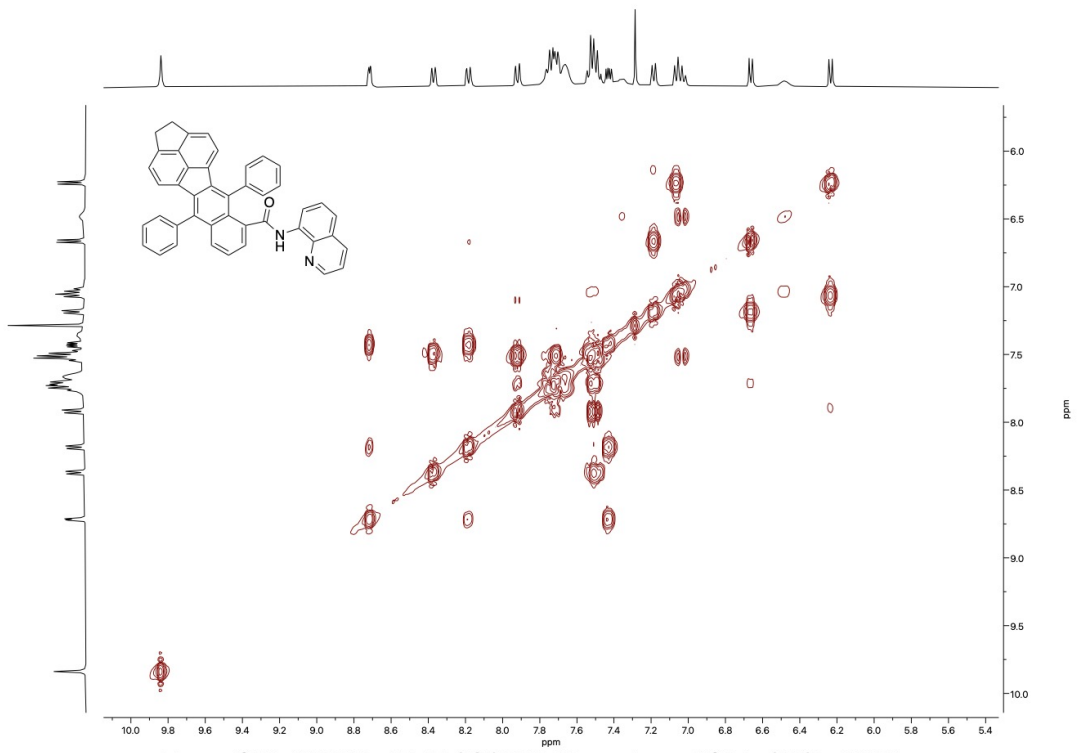

Figure S14: ^{1}H-^{1}H COSY NMR spectrum (400 MHz, $CDCl_3$, 298 K) of G-**2**.

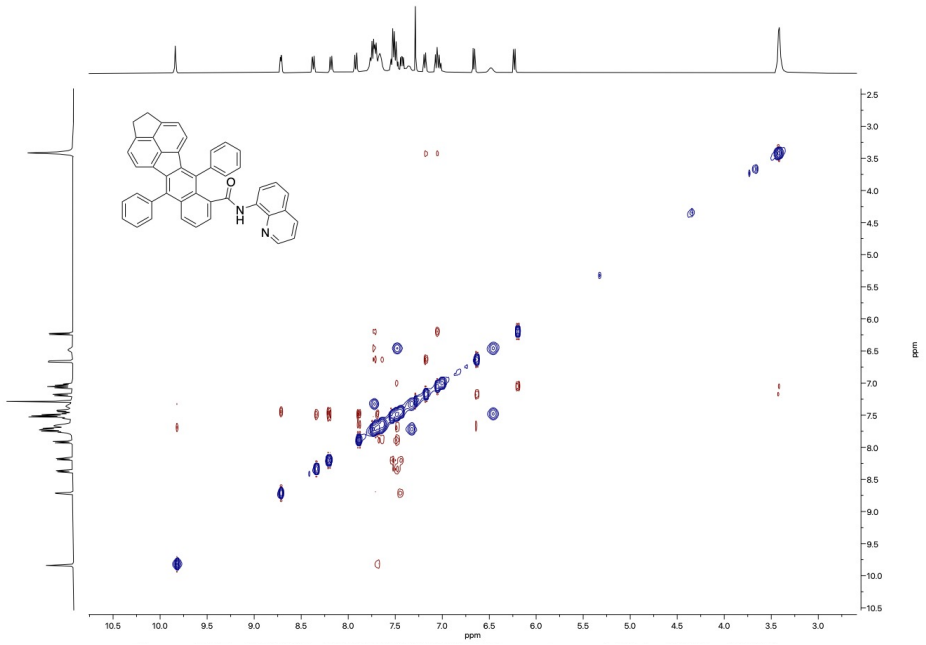

Figure S15: Two-dimensional NOESY NMR spectrum (400 MHz, $CDCl_3$, 298 K) of G-**2**.

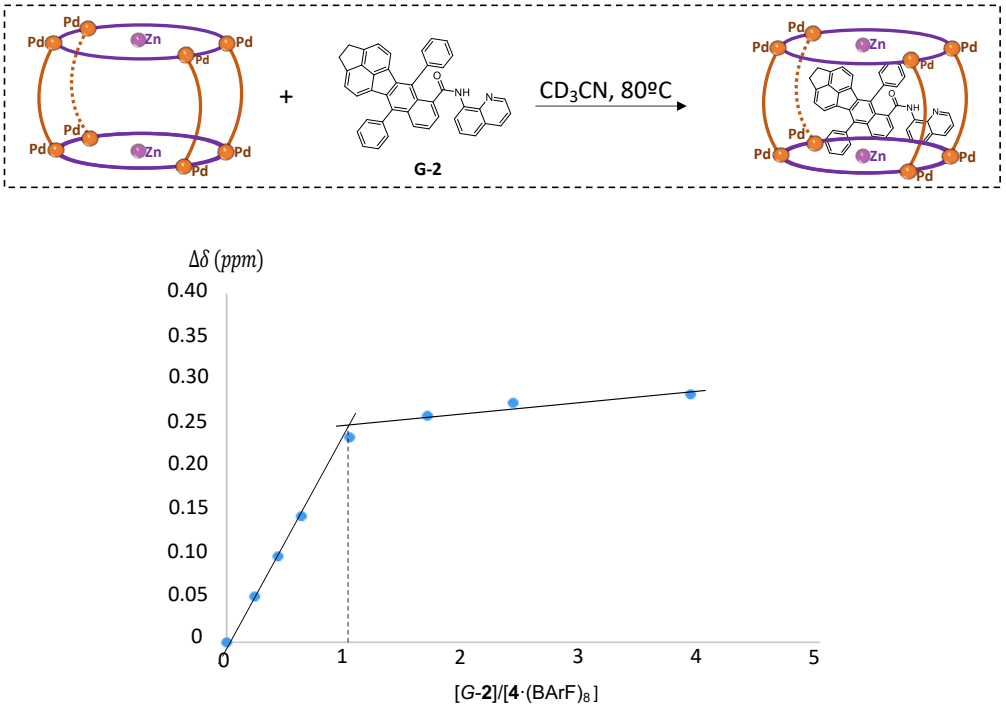

Figure S16. ^{1}H-NMR stoichiometry plot for the titration of **4**·$(BArF)_8$ with G-**2**. A series of 4 mM solutions of **4**·$(BArF)_8$ containing varying concentrations of G-**2**, ranging from 2.06 mM to 66 mM, were prepared. The solutions were allowed to equilibrate before they were examined by ^{1}H-NMR spectroscopy. The stoichiometry was found to be one guest molecule per one host molecule using the mole ratio method.

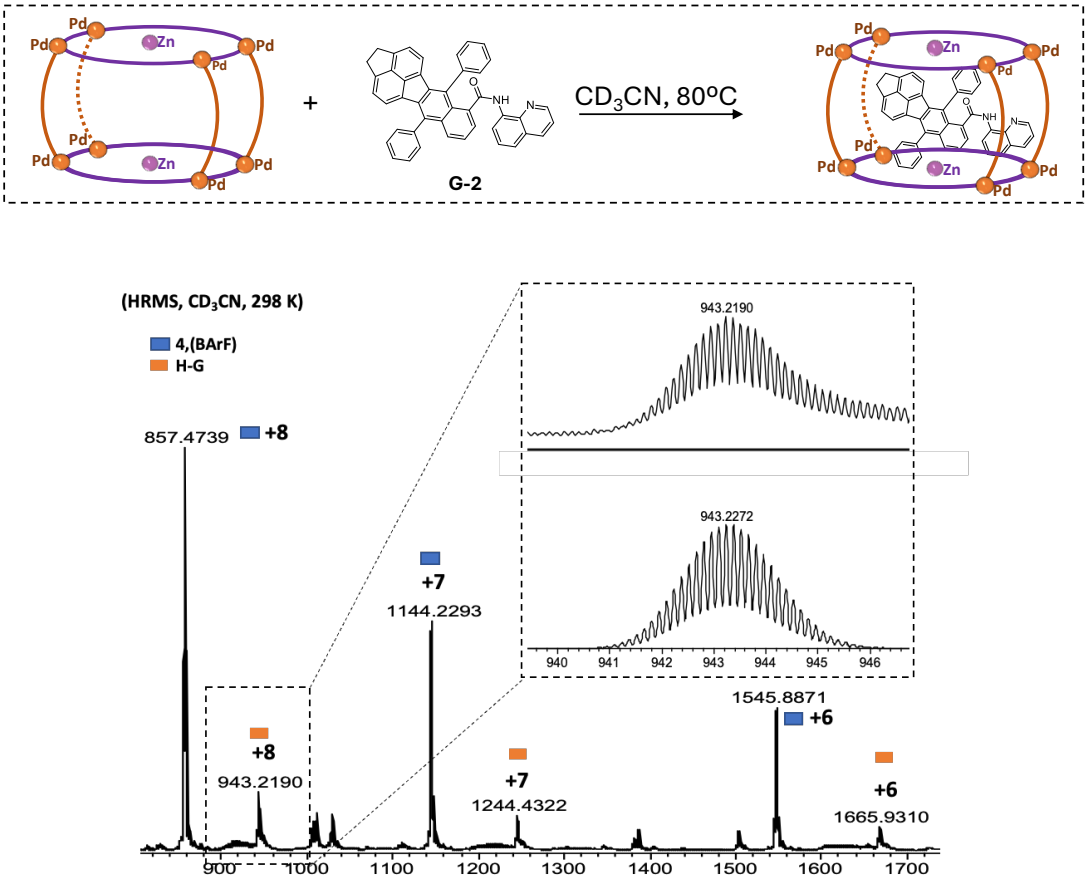

Figure S17: High Resolution Mass Spectrometry (HRMS) spectrum of G-**2** ⊂ **4**·$(BArF)_8$ host-guest complex (CH_3CN solvent).

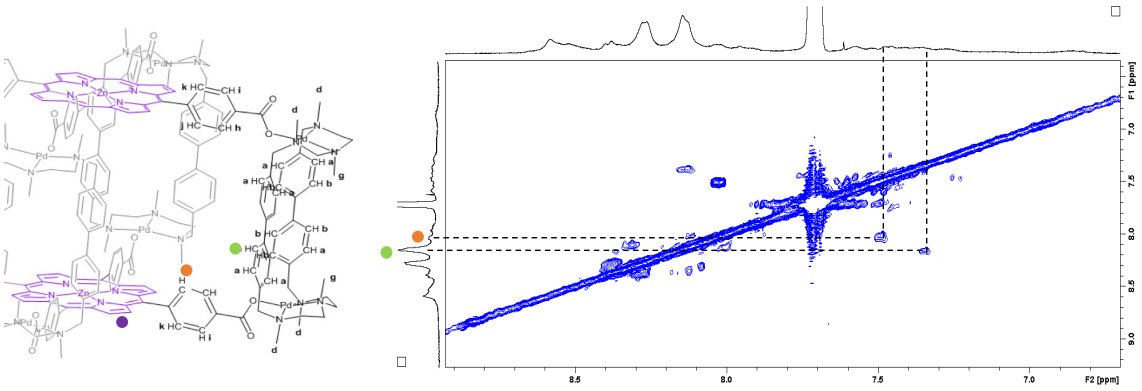

Figure S18. *Two-dimensional NOESY spectra (400 MHz, CD_3CN, 298 K) of G-***2** ⊂**4**·$(BArF)_8$ *host-guest complex. Illustration of different* **4**·$(BArF)_8$ *protons showing NOESY correlations. The correlations observed are attributed to the proximity of the aromatic protons of G-***2** *and the aromatic protons of* **4**·$(BArF)_8$ *pointing inwards towards the host cavity.*

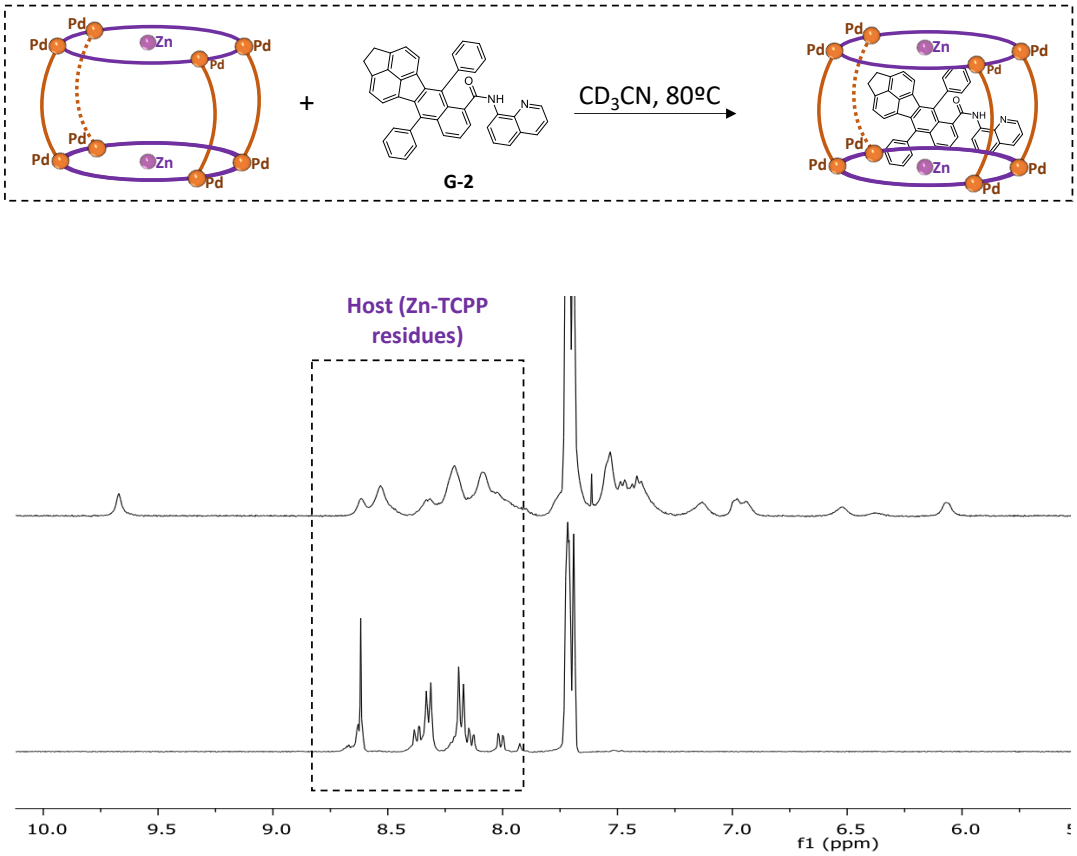

Figure S19: Stacked ^{1}H NMR spectra (400 MHz, CD_3CN) of **4**·$(BArF)_8$ (bottom) and G-**2** ⊂ **4**·$(BArF)_8$ host-guest complex (top).

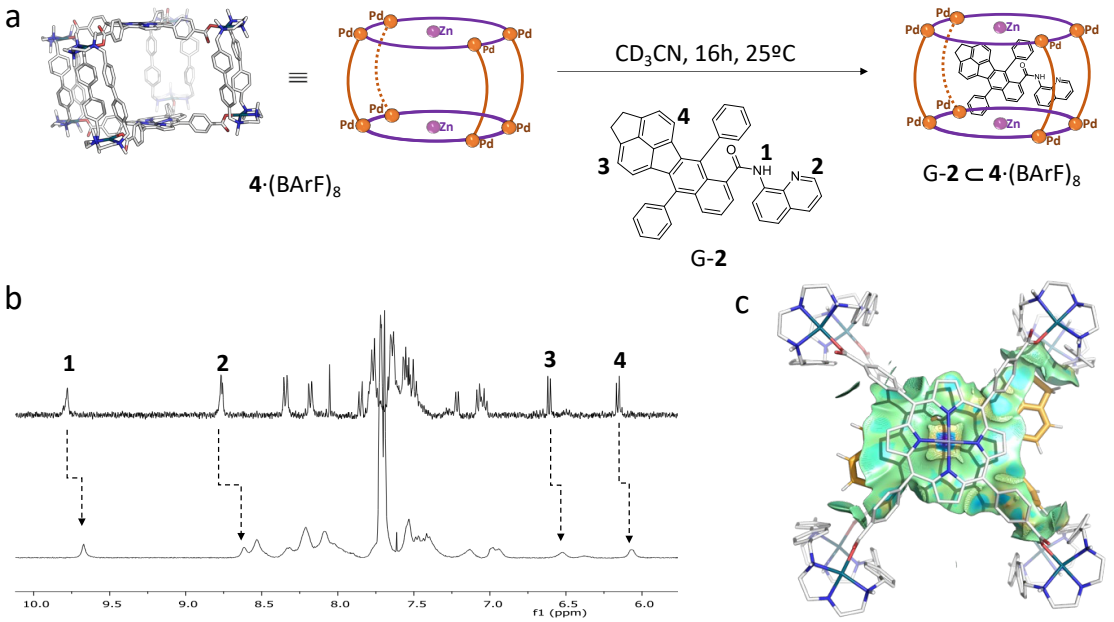

Figure S20: a) Schematic representation of the binding of G-**2** within **4**·(BArF)$_8$. (b) Stacked partial ^{1}H NMR spectra of G-**2** (top) and G-**2** ⊂ **4**·(BArF)$_8$ (bottom), showing spectral changes upon host-guest complexation. (c) Representation of non-covalent interaction (NCI) surface of encapsulated G-**2** within the cage (weak van der Waals interactions in green and stronger interactions in blue).

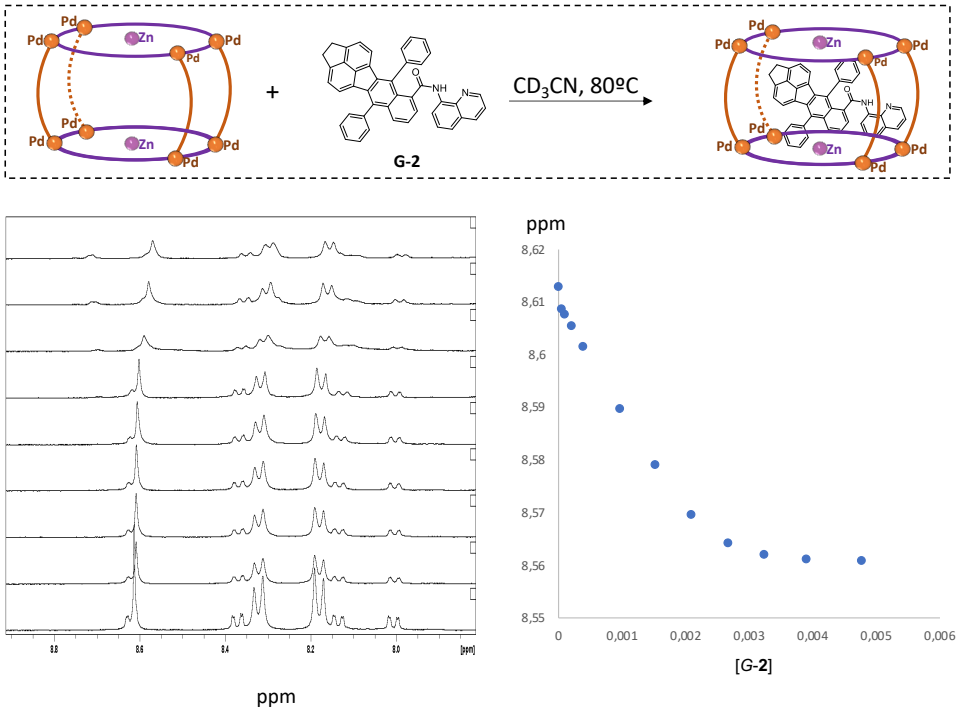

Figure S21: ^{1}H NMR (400 MHz, CD_3CN) monitoring for the titration of **4**·(BArF)$_8$ with G-**2**. Fixed total concentration of **4**·(BArF)$_8$ in acetonitrile was measured to be $8.57 \cdot 10^{-4}$ M (fitting with www.supramolecular.org, K_a = 5.41 (±0.1) × 10^4 M^{-1}). Inset: chemical shift variation of the host plotted versus the different stoichiometries of G-**2**.

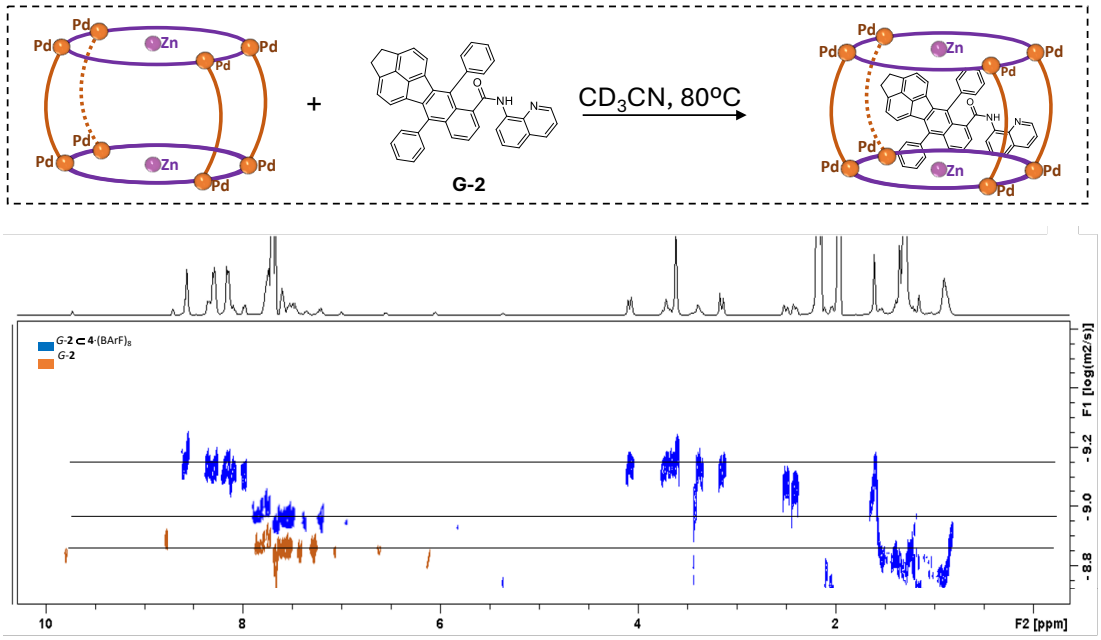

Figure S22: Overlapped ^{1}H DOSY spectra (400 MHz, CD_3CN, 298 K) of the prepared G-**2** ⊂ **4**·$(BArF)_8$ host-guest complex (blue) and the G-**2** (orange). The diffusion coefficients for the host and the guest species in CD_3CN were measured to be $D=10^{-9.157}$ m^2 $s^{-1}$and $D=10^{-8.985}$ m^2 $s^{-1,}$ respectively. The diffusion coefficient for free G-**2** in CD_3CN was measured to be $D=10^{-8.879}$ m^2 s^{-1}. The differences observed in the diffusion coefficients of the guest in the host-guest complex and the free guest are indicative of the confinement of G-**2** within **4**·$(BArF)_8$.

G-**1**

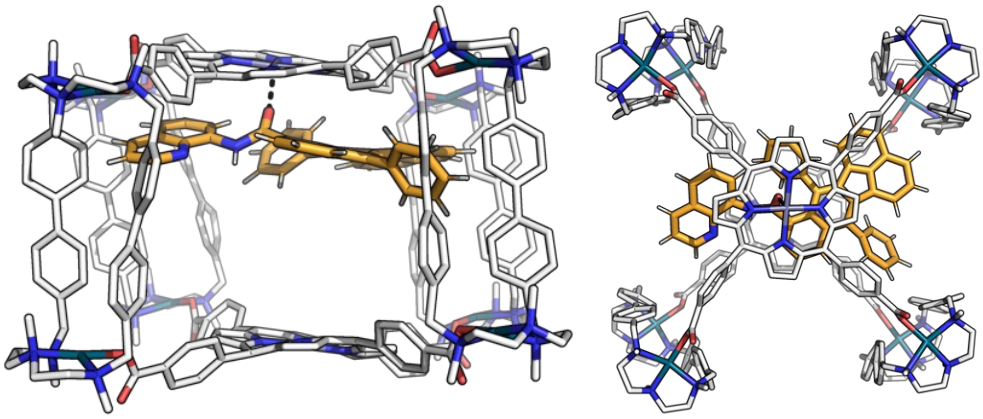

G-**2**

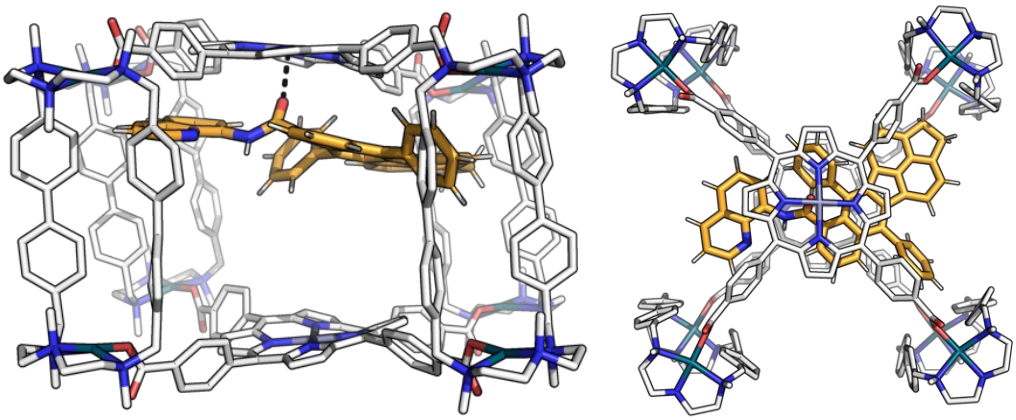

Figure S23: Orientations adopted of G-**1** and G-**2** inside the cage **4**·Cl_8 during MD simulations (3 replicates of 0.5 μs) viewed from the top and from the side. Zn···O interaction is marked with a black dotted line.

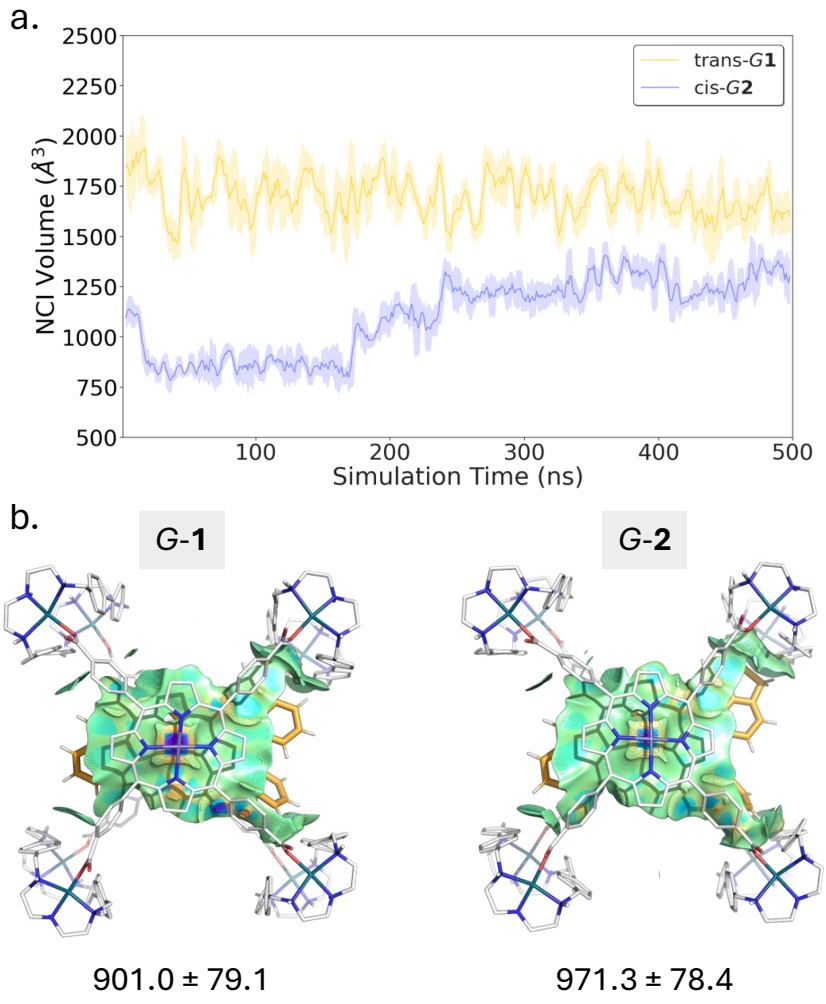

Figure S24: a) Calculated NCI volumes versus the simulation time over one replicate of G-**1** ⊂ **4**·$(BArF)_8$ and G-**2** ⊂ **4**·$(BArF)_8$. b) Representation of NCI surface of G-**1** and G-**2** within the host cavity, with the average NCI volume (in $Å^3$). Visualization of the NCI surface using a rainbow scale with Weak van der Waals interactions represented in green and stronger interactions in blue. Gradient isosurface with s = 0.8 a.u.

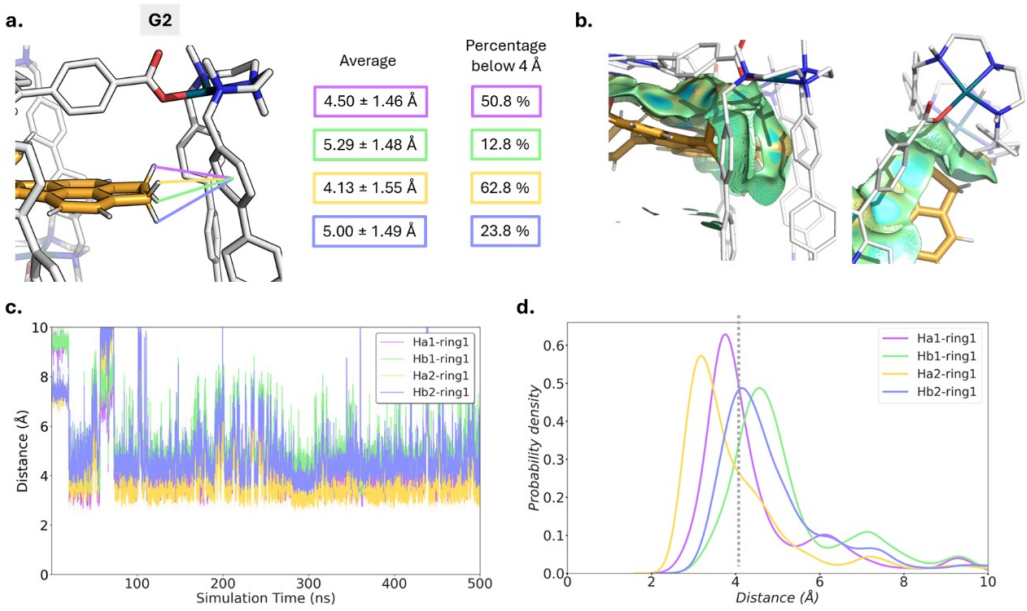

Figure S25: a) Representation of CH-π interactions between the CH_2 groups of G-2 and the phenyls on the clips of the cage with the average distances in Å and the percentage of time when each distance is below 4 Å. b) NCI surface showing van der Waals interactions in green between the CH_2 groups and the phenyl rings of the clips. c) Plotting of the distance between each H atom and the center of the phenyl ring versus the simulation time. d) Histogram of the distance between each H atom and the center of the phenyl ring, showing distances below 4 Å for two H atoms most of the time (in yellow and purple).

V. Characterization of cis/trans-G-3 ⊂ 4·(BArF)$_8$ host-guest complex

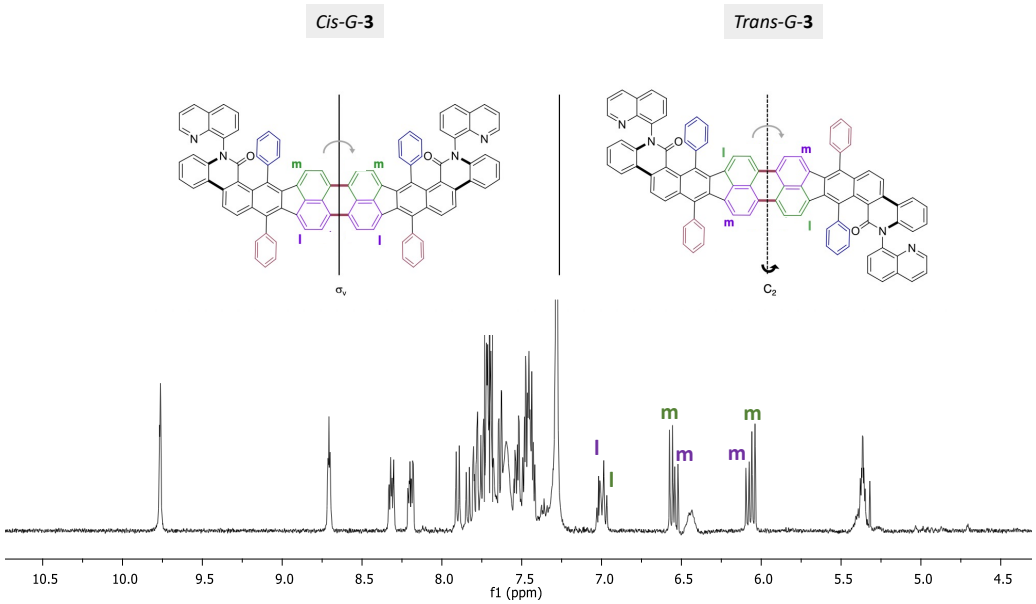

Figure S26: ^{1}H NMR spectrum (400 MHz, $CDCl_3$, 298 K) of *cis*/*trans*-G-**3** isomeric mixture.

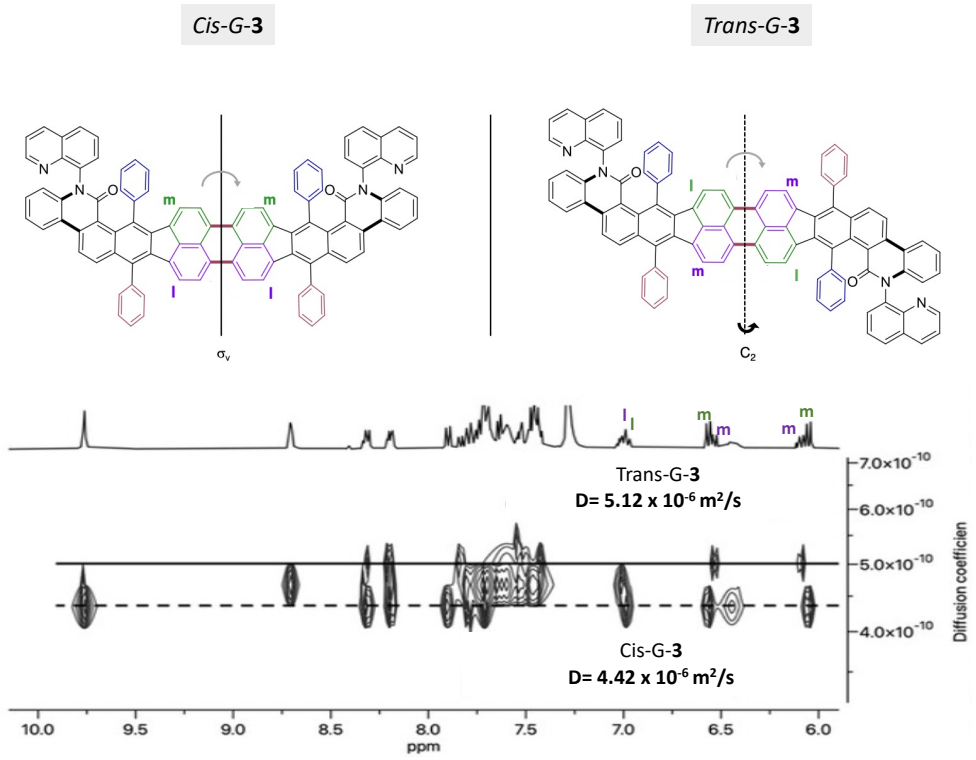

Figure S27: ^{1}H DOSY spectra (400 MHz, $CDCl_3$, 298 K) of *cis*/*trans*-G-**3** isomeric mixture. The diffusion coefficients were measured to be D=5.12x10^{-6}m^2 s^{-1} for *trans*-G-**3** and D=4.42x10^{-6}m^2 s^{-1} for the *cis*/*trans*-G-**3**.

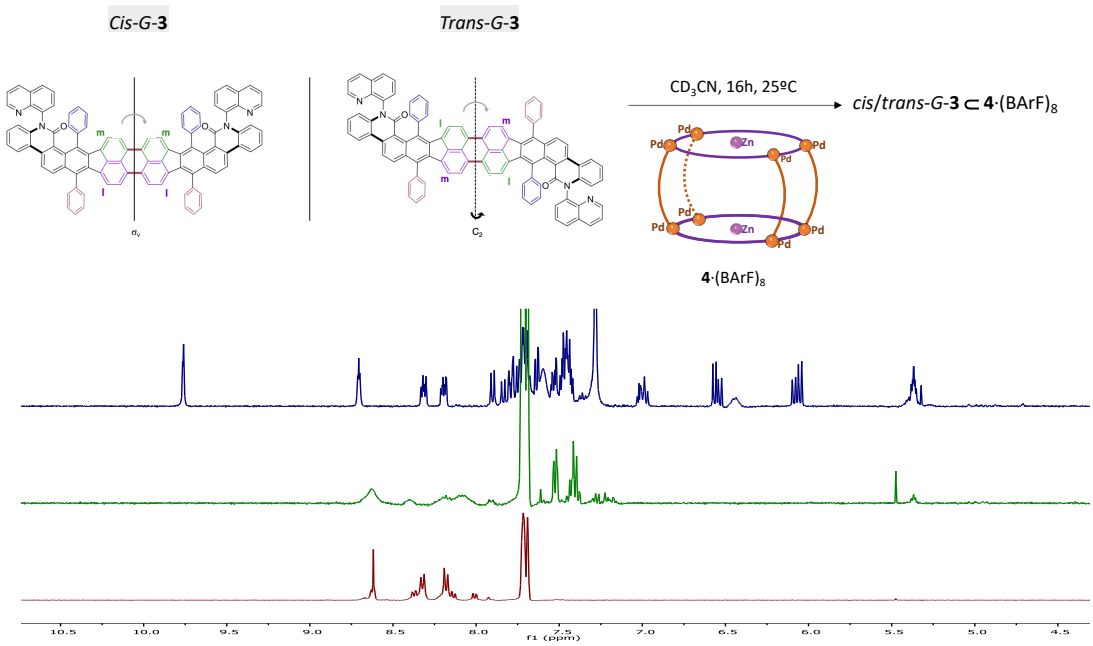

Figure S28: Stacked ^{1}H NMR spectra (400 MHz, CD_3CN, 298 K) of **4**·$(BArF)_8$ (bottom), the prepared *cis*/*trans*-G-**3** ⊂ **4**·$(BArF)_8$ host-guest complex (middle) and *cis*/*trans*-G-**3** (top).

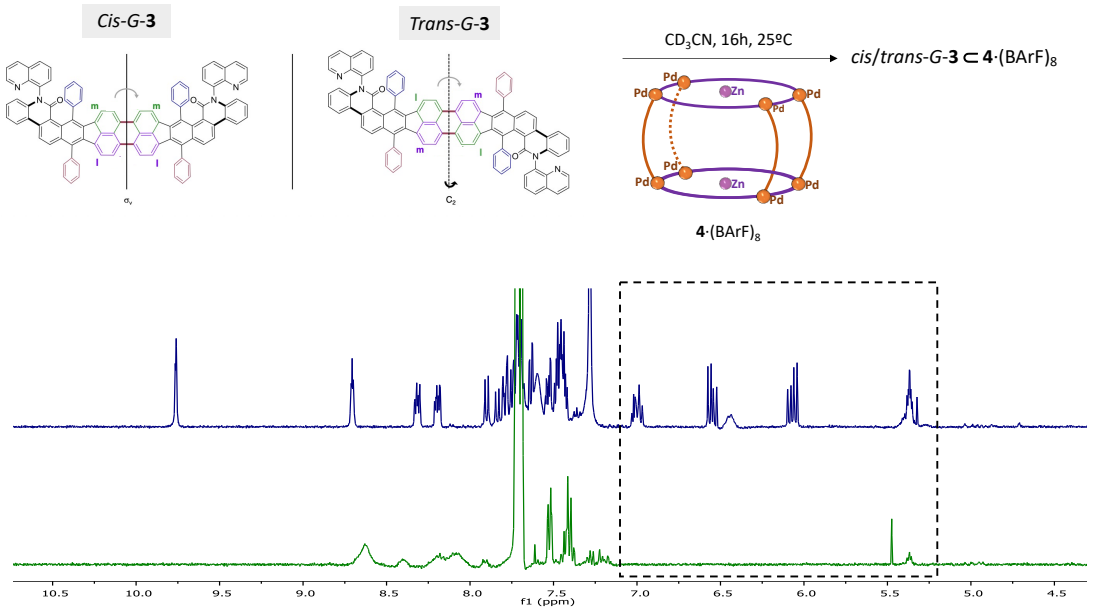

Figure S29: Stacked ^{1}H NMR spectra (400 MHz, CD_3CN, 298 K) of the *cis*/*trans*-G-**3** ⊂ **4**·$(BArF)_8$ host-guest complex (bottom) and *cis*/*trans*-G-**3** (top), highlighting the region from 5-7 ppm.

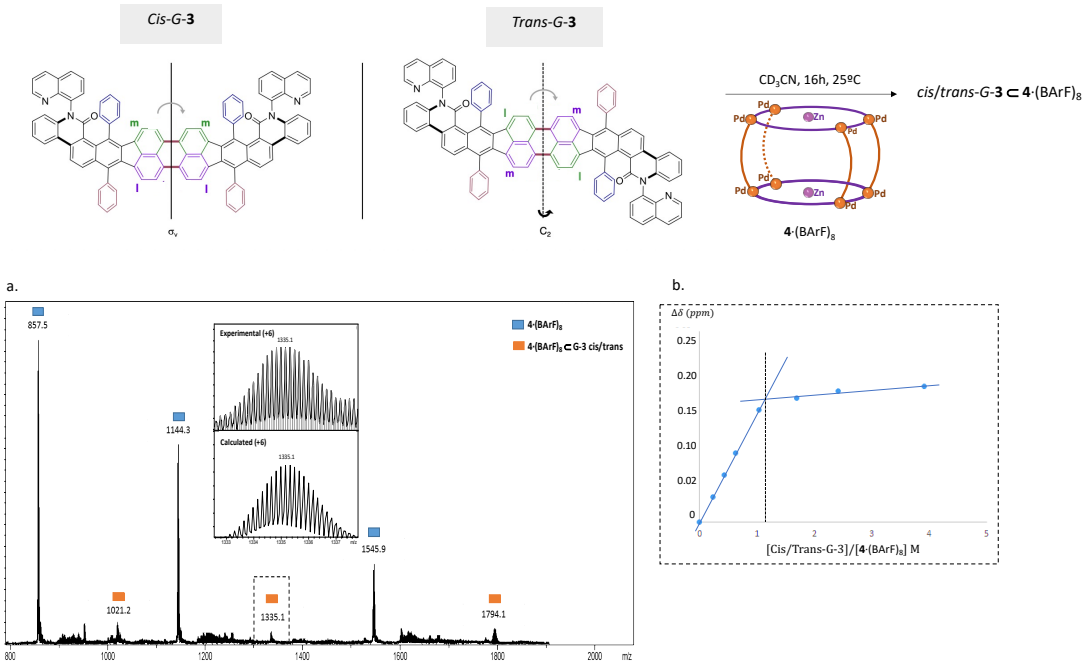

Figure S30: a) High Resolution Mass Spectrometry (HRMS) spectrum of cis/trans-G-**3** ⊂ **4**·$(BArF)_8$ host-guest complex (CH_3CN solvent) and selected peak (+6) isotopic pattern comparison between experimental and calculated. b) ^{1}H-NMR stoichiometry plot for the titration of **4**·$(BArF)_8$ with cis/trans-G-**3**.

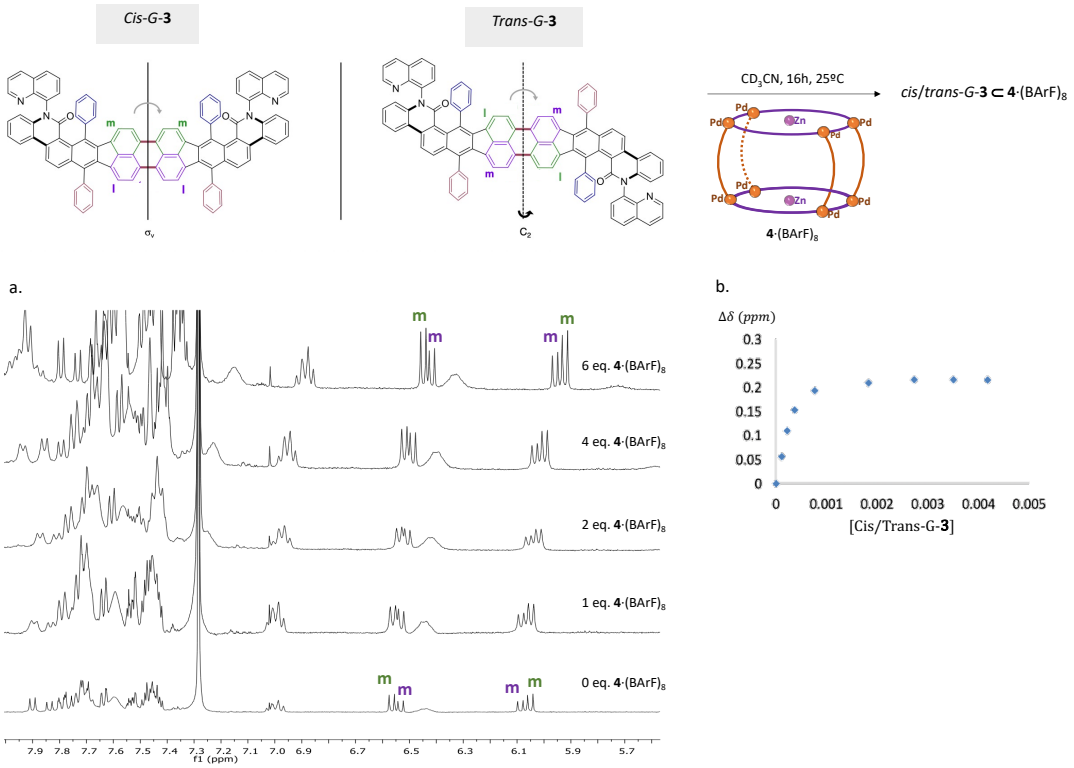

Figure S31: a) ^{1}H NMR (400 MHz, CD_3CN) monitoring for the titration of cis/trans-G-**3** with **4**·$(BArF)_8$. Fixed total concentration of cis/trans-G-**3** mixture in acetonitrile was measured to be $2.10 \cdot 10^{-4}$ M. b) fitting with www.supramolecular.org, K_a = 1.32 (±0.1) × 10^5 M^{-1}.

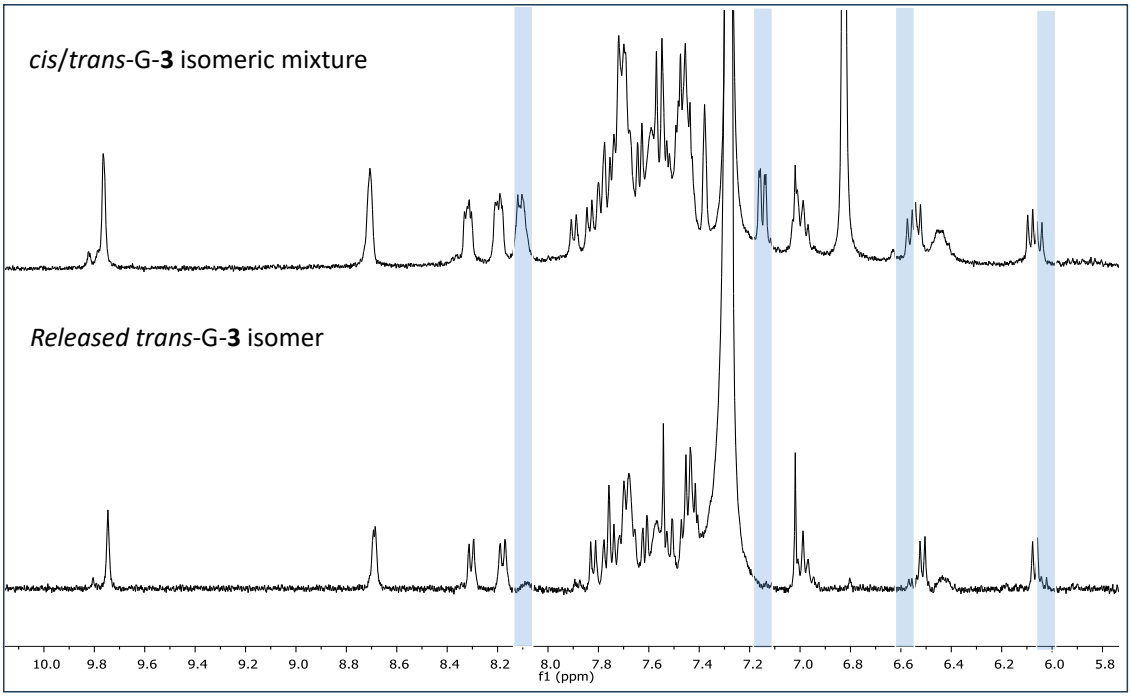

Figure S32: Stacked ^{1}H NMR spectra (400 MHz, CD_3CN, 298 K) of *cis*/*trans*-G-**3** isomeric mixture (top) and purified trans-G-**3** released from *trans*-G-**3** ⊂ **4**·$(BArF)_8$ host-guest complex formed in the biphasic system (bottom).

*trans-G-***3**

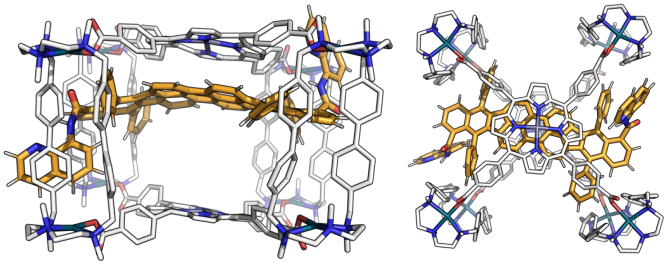

*cis-G-***3**

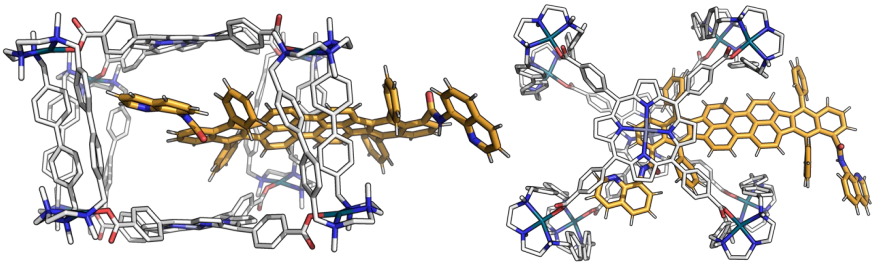

Figure S33: Orientations adopted of *trans*-G-**3** and *cis*-G-**3** inside the cage **4**·Cl_8 during MD simulations (3 replicates of 0.5 μs) view from the top and from the side.

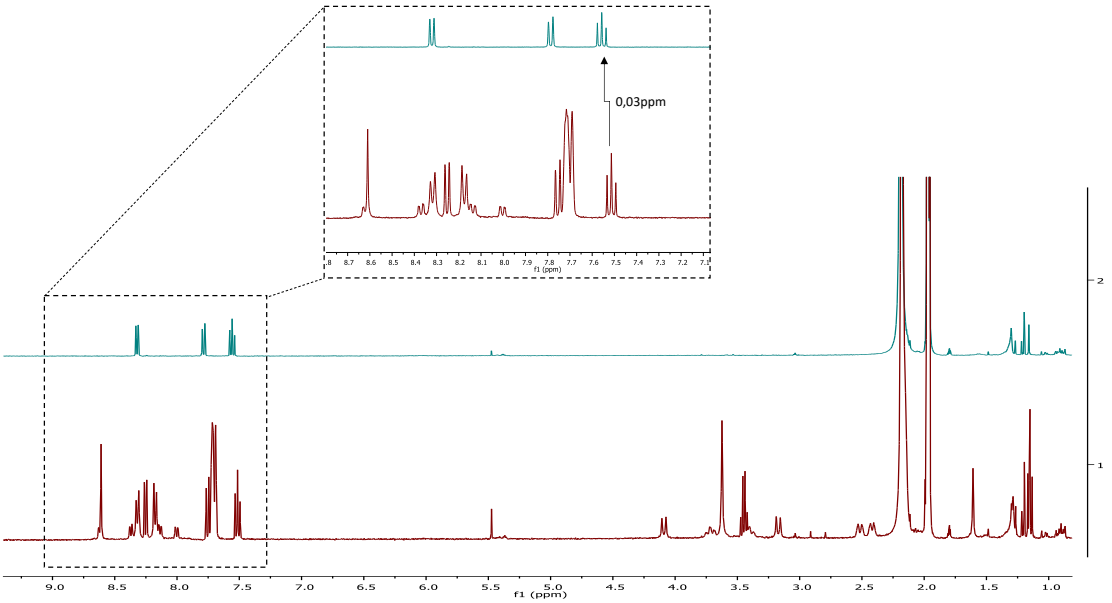

Figure S34. *Stacked ^{1}H NMR spectra (400 MHz, CD_3CN) of Perylene⊂**4**·$(BArF)_8$ host-guest complex (bottom) and perylene (top).*

VI. References

1. L. Capdevila, J. Sala, C. Berga, A. de Aquino, T. Parella, L. Blancafort, L. Rodríguez, S. Simon and X. Ribas, *ChemistryEurope*, 2025, **3**, e202500102.

2. C. García-Simón, M. Garcia-Borràs, L. Gómez, T. Parella, S. Osuna, J. Juanhuix, I. Imaz, D. Maspoch, M. Costas and X. Ribas, *Nat. Commun.*, 2014, **5**, 5557.

3. C. García-Simón, C. Colomban, Y. A. Çetin, A. Gimeno, M. Pujals, E. Ubasart, C. Fuertes-Espinosa, K. Asad, N. Chronakis, M. Costas, J. Jiménez-Barbero, F. Feixas and X. Ribas, *J. Am. Chem. Soc.*, 2020, **142**, 16051-16063.

4. J. Wang, R. M. Wolf, J. W. Caldwell, P. A. Kollman and D. A. Case, *J. Comput. Chem.*, 2004, **25**, 1157-1174.

5. P. Li and K. M. Merz, Jr., *J. Chem. Inf. Model.*, 2016, **56**, 599-604.

6. C. I. Bayly, P. Cieplak, W. Cornell and P. A. Kollman, *J. Chem. Phys.*, 1993, **97**, 10269-10280.

7. M. J. T. Frisch, G. W.; Schlegel, H. B.; Scuseria, G. E.; Robb, M. A.; Cheeseman, J. R.; Scalmani, G.; Barone, V.; Petersson, G. A.; Nakatsuji, H.; Li, X.; Caricato, M.; Marenich, A. V.; Bloino, J.; Janesko, B. G.; Gomperts, R.; Mennucci, B.; Hratchian, H. P.; Ortiz, J. V.; Izmaylov, A. F.; Sonnenberg, J. L.; Williams-Young, D.; Ding, F.; Lipparini, F.; Egidi, F.; Goings, J.; Peng, B.; Petrone, A.; Henderson, T.; Ranasinghe, D.; Zakrzewski, V. G.; Gao, J.; Rega, N.; Zheng, G.; Liang, W.; Hada, M.; Ehara, M.; Toyota, K.; Fukuda, R.; Hasegawa, J.; Ishida, M.; Nakajima, T.; Honda, Y.; Kitao, O.; Nakai, H.; Vreven, T.; Throssell, K.; Montgomery, J. A., Jr.; Peralta, J. E.; Ogliaro, F.; Bearpark, M. J.; Heyd, J. J.; Brothers, E. N.; Kudin, K. N.; Staroverov, V. N.; Keith, T. A.; Kobayashi, R.; Normand, J.; Raghavachari, K.; Rendell, A. P.; Burant, J. C.; Iyengar, S. S.; Tomasi, J.; Cossi, M.; Millam, J. M.; Klene, M.; Adamo, C.; Cammi, R.; Ochterski, J. W.; Martin, R. L.; Morokuma, K.; Farkas, O.; Foresman, J. B.; Fox, D. J. , *Journal*, 2016.

8. R. Salomon-Ferrer, A. W. Götz, D. Poole, S. Le Grand and R. C. Walker, *J. Chem. Theory Comput.*, 2013, **9**, 3878-3888.

9. I. Y. B.-S. D.A. Case, S.R. Brozell, D.S. Cerutti, T.E. Cheatham, III, V.W.D. Cruzeiro, T.A. Darden, R.E. Duke, D. Ghoreishi, M.K. Gilson, H. Gohlke, A.W. Goetz, D. Greene, R Harris, N. Homeyer, Y. Huang, S. Izadi, A. Kovalenko, T. Kurtzman, T.S. Lee, S. LeGrand, P. Li, C. Lin, J. Liu, T. Luchko, R. Luo, D.J. Mermelstein, K.M. Merz, Y. Miao, G. Monard, C. Nguyen, H. Nguyen, I. Omelyan, A. Onufriev, F. Pan, R. Qi, D.R. Roe, A. Roitberg, C. Sagui, S. Schott-Verdugo, J. Shen, C.L. Simmerling, J. Smith, R. SalomonFerrer, J. Swails, R.C. Walker, J. Wang, H. Wei, R.M. Wolf, X. Wu, L. Xiao, D.M. York and P.A. Kollman *University of California, San Francisco*, 2018.

10. J. Contreras-García, E. R. Johnson, S. Keinan, R. Chaudret, J.-P. Piquemal, D. N. Beratan and W. Yang, *J. Chem. Theory Comput.*, 2011, **7**, 625-632.

11. R. A. Boto, F. Peccati, R. Laplaza, C. Quan, A. Carbone, J.-P. Piquemal, Y. Maday and J. Contreras-García, *J. Chem. Theo. Comput.*, 2020, **16**, 4150-4158.